

DNS STUDY ON VISCOELASTIC EFFECT IN DRAG-REDUCED TURBULENT
CHANNEL FLOW

Takahiro Ishigami, Takahiro Tsukahara, Yasuo Kawaguchi

Department of Mechanical Engineering,
Tokyo University of Science
Yamazaki 2641, Noda-shi, Chiba 278-8510, Japan
tsuka@rs.noda.tus.ac.jp

Bo Yu

Department of Mechanical Engineering,
Beijing University of Petroleum
Changping, Beijing 102200, China

ABSTRACT

An investigation on mechanisms of the turbulent drag reduction, induced by the viscoelasticity of non-Newtonian fluids, is in progress. In the present work, the effects of viscoelastic contribution is examined by direct numerical simulations (DNS), using the Giesekus model for surfactant solutions. A series of DNS on the turbulent channel flow has been performed for different rheological properties, with respect to Weissenberg number and the ratio of solvent contribution to the total zero-shear viscosity, at different Reynolds numbers. It is found that high drag reduction can be achieved by suppression of the turbulent production for high Weissenberg number, and/or by decrease of the effective viscosity irrespective of the Reynolds number. Moreover, we focus on the viscoelastic contribution term in the budget of Reynolds stresses and its relation to the local flow pattern.

INTRODUCTION

It is well known that the small amount of polymers or surfactant additives to flowing liquid give rise to drag reduction (DR) in a wall-bounded turbulent flow. In the past six decades since the discovery of Toms effect (1948), a number of works have been done to investigate this phenomenon and to apply it to practical applications. One of the most successful applications of this effect was that in the Trans-Alaska pipeline, in which the desired discharge of an additional million barrels of crude oil per day was accomplished by the addition of polymers. However, because of the difficulty in analysing the interaction between additives and turbulent motions at the molecular level, the mechanism of drag-reducing turbulent flow by surfactant additives has not been satisfactorily clarified. This is partly due to the limitation of present experimental facilities, with which it is extremely difficult to measure various instantaneous quantities such as velocity and pressure in the vicinity of the walls with sufficient accuracy. A direct numerical simulation (DNS) has become an important tool to study physics of turbulence and can identify instantaneous structures in turbulence. Recently, DNS has been used to study drag-reducing flow by additives (e.g., Sureshkumar *et al.*, 1997; Den Toonder *et al.*, 1997; Dimitropoulos *et al.*, 1998; Housiadas & Beris, 2004), and it was found that a viscoelastic model can reproduce most of the experimental observations (such as wider buffer layer, reduction of Reynolds shear stress and larger spacing between low-speed streaks).

Although there are competing models (e.g., FENE-P, Oldroyd-B), the Giesekus model, proposed by Giesekus (1982), is adopted in our study because this model can describe well the measured apparent shear viscosity and extensional viscosity of the surfactant solution: cf. Wei *et al.* (2006). On the other hand, the FENE-P model was already shown to be able to reproduce the essential effect of polymers and provide evidence that polymers disrupt the near-wall turbulence regeneration cycle and reduce the turbulent friction drag (see, e.g., White & Mungal (2008)). As for the surfactant additives, Suzuki *et al.* (2001) studied numerically the drag-reducing flow with using a Giesekus model. The author's group (Yu & Kawaguchi, 2004, 06; Yu *et al.*, 2004) has simulated a viscoelastic fluid by DNS with the Giesekus model. The numerical results are qualitatively agreed with experimental data, indicating that this model is appropriate for surfactant solutions. In this study, we considered dilute surfactant solutions, in which the shear-thinning behavior was assumed to be negligible and the elongational viscoelastic effect was taken into account using various methods for the extra elastic stresses.

The present objectives are to perform DNS of the drag-reducing flow with surfactant additives, and to examine the role and influence of the viscoelasticity in drag-reducing effect on the structures of wall-bounded turbulent shear flow.

NOMENCLATURE

\mathbf{A}	: velocity-gradient tensor = $\partial u_i / \partial x_j$
C_f	: skin friction coefficient = $2\tau_w / \rho u_m^2$
c_{ij}	: conformation tensor
$DR\%$: drag-reduction rate
p	: pressure
Re_m^*	: Reynolds number = $2\rho u_m \delta / \eta_{eff}$
Re_τ	: Reynolds number = $\rho u_\tau \delta / \eta_0$
t	: time
u, v, w	: velocity component in $x, y,$ or z direction
u_m	: bulk mean velocity
u_τ	: friction velocity = $\sqrt{\tau_w / \rho}$
We_τ	: Weissenberg number = $\rho \lambda u_\tau^2 \delta / \eta_0$
x_1, x	: streamwise direction
x_2, y	: wall-normal direction
x_3, z	: spanwise direction
Greek	
α	: mobility factor
β	: ratio = η_s / η_0

Table 1: Computational parameters and important results.

Fluid	(We_τ, β)	u_m^+	η_0/η_{eff}	Re_m^*	$DR\%$
A	(0, 1.0)	15.2	1.00	4570	—
B1	(30, 0.5)	25.9	1.45	11300	58.1
B2	(30, 0.5)	29.6	1.45	33800	57.6
C	(30, 0.3)	29.6	1.93	17200	64.2
D	(40, 0.5)	30.1	1.53	13800	67.1
E	(10, 0.8)	16.3	1.04	5110	13.2
F	(10, 0.5)	17.1	1.13	5750	18.0
G1	(11, 0.5)	20.8	1.15	6130	26.1
G2	(11, 0.5)	21.0	1.15	19100	29.3

- δ : channel half width
- δ_{ij} : Kronecker delta
- ε : dissipation rate
- η_0 : viscosity of the surfactant solution at zero-shear rate = $\eta_a + \eta_s$
- η_a : shear viscosity of surfactant contribution
- η_{eff} : effective viscosity at the wall
- η_s : shear viscosity of solvent contribution
- λ : relaxation time
- τ_w : mean wall shear stress
- ρ : density
- Superscript and subscript
- $()^*$: normalized by u_τ, ρ, δ
- $()^+$: normalized by u_τ, ρ, η_0
- $()_\eta$: normalized by $u_\tau, \rho, \eta_{\text{eff}}$
- $()'$: fluctuation component
- $()$: statistically averaged
- $()_{\text{rms}}$: root-mean-square value

NUMERICAL PROCEDURE

A series of DNS on a turbulent plane channel flow have been performed at friction Reynolds numbers of $Re_\tau = 150$ and 395. We employed a viscoelastic Giesekus constitutive equation to calculate the extra stress caused by the interaction between shear rate and the elasticity network structure of surfactant additives. The dimensionless governing equations for fully developed viscoelastic turbulent channel flow can be written as follows: the continuity equation

$$\frac{\partial u_i^+}{\partial x_i^*} = 0, \quad (1)$$

the Navier-Stokes equation

$$\begin{aligned} \frac{\partial u_i^+}{\partial t^*} + u_j^+ \frac{\partial u_i^+}{\partial x_j^*} = & -\frac{\partial p^+}{\partial x_i^*} + \frac{\beta}{Re_\tau} \frac{\partial}{\partial x_j^*} \left(\frac{\partial u_i^+}{\partial x_j^*} \right) \\ & + \frac{(1-\beta)}{We_\tau} \frac{\partial c_{ij}^+}{\partial x_j^*} + \delta_{1i}, \end{aligned} \quad (2)$$

and the constitutive equation

$$\begin{aligned} \frac{\partial c_{ij}^+}{\partial t^*} + \frac{\partial u_k^+ c_{ij}^+}{\partial x_k^*} - \frac{\partial u_i^+ c_{kj}^+}{\partial x_k^*} - \frac{\partial u_j^+ c_{ki}^+}{\partial x_k^*} \\ = -\frac{Re_\tau}{We_\tau} [c_{ij}^+ - \delta_{ij} + \alpha (c_{ik}^+ - \delta_{ik}) (c_{kj}^+ - \delta_{kj})], \end{aligned} \quad (3)$$

where c_{ij} is the conformation tensor associated with deformation of network structures. The mobility factor, which is a parameter determining the extensional viscosity, is set to be $\alpha = 0.001$.

Table 2: Reynolds number and Computational domain size; L_i, N_i and Δi are box length, grid number and spatial resolution in i -direction.

Fluid	A	B1, C, D, E, F, G1	B2, G2
L_x^*, L_z^*	10.0, 5.0	12.8, 6.4	12.8, 6.4
N_x, N_z	128, 128	128, 128	256, 256
N_y	128	128	256
$\Delta x^*, \Delta z^*$	0.08, 0.05	0.10, 0.05	0.05, 0.025
Δy_{min}^*	0.00149	0.00149	0.00075
Δy_{max}^*	0.03013	0.03013	0.01506
Re_τ	150	150	395

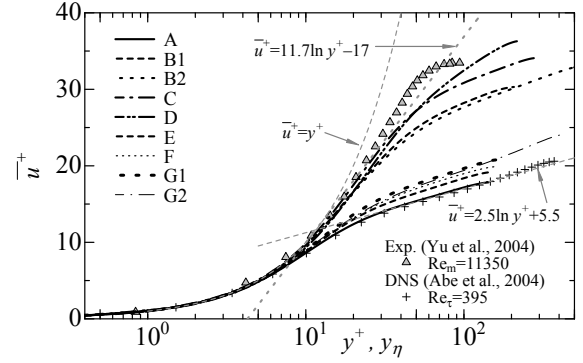


Figure 1: Mean velocity profile in comparison with data from PIV experiment (Yu *et al.*, 2004). Dotted line is the empirical law so-called Virk's ultimate profile (Virk, 1971).

The periodic boundary condition is employed in streamwise and spanwise directions, and the non-slip condition is imposed on the walls. For the spatial discretization, the finite difference method is adopted. The numerical scheme with the 4th-order accuracy is employed in the streamwise and spanwise directions, and the 2nd-order accuracy is applied in the wall-normal direction. The 2nd-order MINMOD scheme is adopted to the convective term in the constitutive equation. Time advancement is done by the 2nd-order Adams-Bashforth method, but the 2nd-order Crank-Nicolson method is used for the viscous terms in the wall-normal direction.

We investigated effects of the various rheological parameters on the drag reduction. Table 1 summarizes the important flow parameters of the non-Newtonian fluid as well as mean flow variables, such as the actual bulk Reynolds number Re_m . In addition, chosen frictional Reynolds numbers are shown in Table 2, in which the computational domain size is also listed.

RESULTS AND DISCUSSION

The mean velocity profiles are plotted in Fig. 1, including the experimental data obtained by Yu *et al.* (2004). In their experiment, a drag-reduction rate $DR\%$ of 51% (defined later) was achieved using surfactant solution of cetyltrimethyl ammonium chloride (CTAC) dissolving in water with a concentration 75 ppm. The DNS result for Newtonian fluid by Abe *et al.* (2004) is also drawn in the figure. Here y_η is the wall-normal height non-dimensionalized by the viscous length based on the effective viscosity at the wall (Sureshkumar *et al.*, 1997), which is obtained as

$$\eta_{\text{eff}} = \eta_0 \left(\beta \frac{du}{dy} + \frac{(1-\beta)c_{xy}}{We_\tau} \right) \bigg/ \frac{du}{dy}. \quad (4)$$

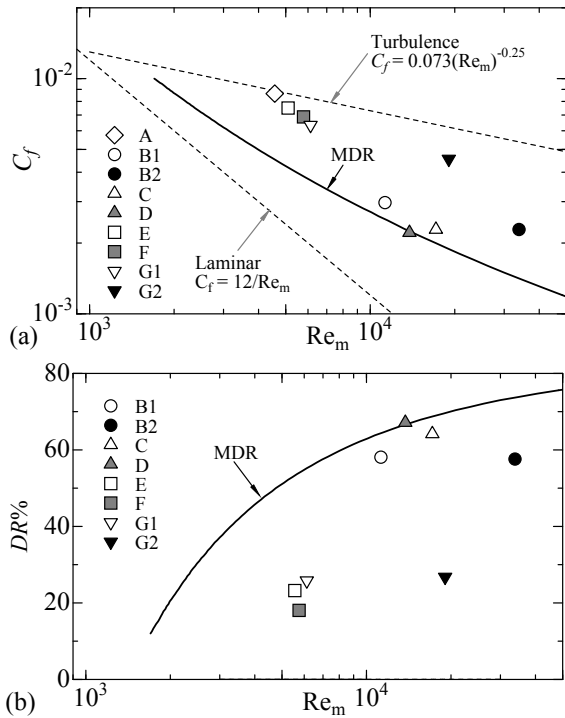


Figure 2: (a) C_f vs Re_m^* , (b) $DR\%$ vs Re_m^* . Solid line is Virk's maximum drag-reduction asymptote (MDR).

The present results are in qualitative agreement with their data. For non-Newtonian fluid, there exists a shift of the logarithmic law of a Newtonian fluid due to the presence of the additives. The magnitude of the shift seems to depend mainly on We_τ . The highest drag-reduction rate in the present study is achieved by fluid D of $We_\tau = 40$, in which no apparent log-law region is found, as shown in Fig. 1. However, the log-law profile for $We_\tau \leq 30$ can be observed from a position higher than that of Newtonian fluid. Though Re_τ increases with the same rheological parameters (fluids B1 and B2, or G1 and G2), the shift displacement of the log-law from the Newtonian profile is almost the same level.

In Table 1, note that Re_m^* is based on η_{eff} , and the drag-reduction rate is defined as

$$DR\% = \frac{(C_f^D - C_f)}{C_f^D} \times 100\% \quad (5)$$

where C_f is the actual value for non-Newtonian fluid and C_f^D is the value estimated by the Dean's empirical correlation (Dean, 1978) for Newtonian fluid at the same bulk Reynolds number. The result indicates that the $DR\%$ increases with the increase of We_τ . For instance, a slight increase of about $We_\tau = 10 \rightarrow 11$ (fluids F to G1) induces a rise of 8% in $DR\%$. Its increment is relatively significant when comparing with fluids B1 to D ($We_\tau = 30 \rightarrow 40$). This is because the C_f and $DR\%$ for fluids B1 and D are close to Virk's MDR asymptote (Virk, 1971) whereas those of fluids F to G1 are approximately turbulence values, as given in Fig. 2. In a high- $DR\%$ flow at high We_τ , the production and redistribution of streamwise velocity fluctuation are suppressed, as discussed later with the budget of turbulent energy $\overline{u'u'}$.

A comparison between fluids B1 and C (or fluids E and F) also indicates that the $DR\%$ increases with the decrease of β at a constant Re_τ . In this case, the effective viscosity of η_{eff} is remarkably decreased, causing a decrease in C_f and an

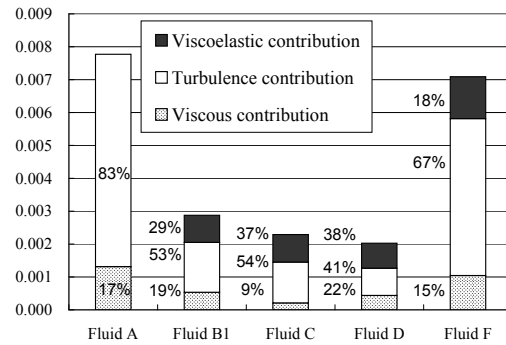


Figure 3: Fractional contribution to friction coefficient.

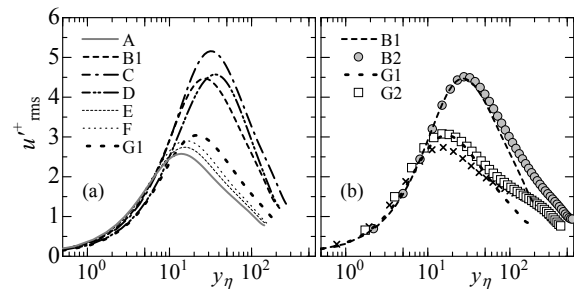


Figure 4: Root-mean-square of streamwise velocity fluctuation u' : (a) various rheological conditions at $Re_\tau = 150$; (b) comparison between $Re_\tau = 180$ and 395. Symbol of \times is the DNS by Abe *et al.* (2004) for Newtonian fluid at $Re_\tau = 395$.

increase in $DR\%$. Therefore we can identify two types of factors in the drag reduction: the decreases of the turbulent production (by increasing We_τ) and of the effective viscosity (by decreasing β). As for the Reynolds-number dependence, a comparison between fluid B1 and B2 (also G1 and G2) indicates that there is no meaningful distinction in $DR\%$ and η_0/η_{eff} .

Fukagata *et al.* (2002) proposed a direct relation between the skin friction coefficient and the Reynolds stress distribution. This identical equation indicates that the skin friction coefficient can be decomposed into the laminar contribution, the turbulent contribution and the inhomogeneous and transient contributions. The equation for the channel flow of a non-Newtonian fluid governed by Eq. (2) is derived as follows,

$$C_f = 12 \frac{\beta}{Re_m} + 6 \int_0^1 \left(-\overline{u'^+ v'^+} \right) \frac{(1-y^*)}{u_m^{+2}} dy^* + 6 \int_0^1 \frac{c_{xy}^+ (1-\beta)}{We_\tau} \frac{(1-y^*)}{u_m^{+2}} dy^*. \quad (6)$$

The first term is the laminar contribution, the second term is the turbulent contribution and the third term is viscoelastic contribution. For five typical cases, the fractional contribution made by each part is shown in Fig. 3. The reduction of skin friction coefficient of non-Newtonian fluid is attributed mainly to the remarkable reduction of the turbulence contribution, though the additional viscoelastic contribution is small but not trivial. It is worth noting that, although fluids C and D yield almost the same high $DR\%$, the former gives a smaller laminar contribution and a larger turbulence contribution than those of latter case. As mentioned before, the low β for fluid C induces a decrease of the laminar contribution, and the high We_τ for fluid D damps down the turbulence contribution.

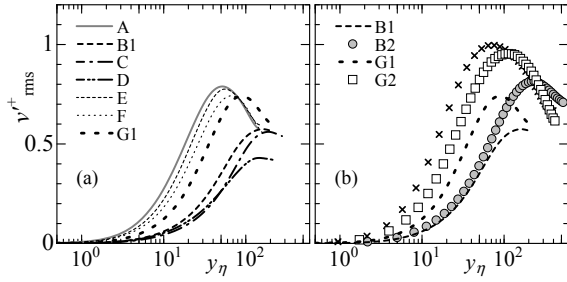


Figure 5: Same as Fig. 4 but for v' .

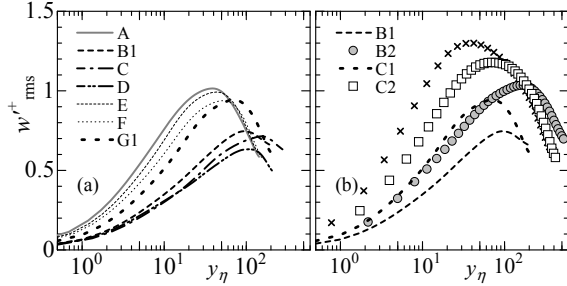


Figure 6: Same as Fig. 4 but for w' .

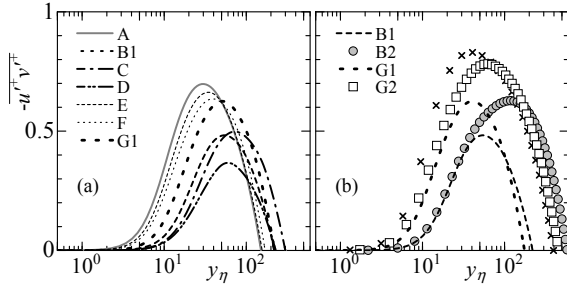


Figure 7: Same as Fig. 4 but for $-u'+v'+$.

Figures 4–6 show the turbulent intensities. It can be found that, for high- $DR\%$ cases, u'_{rms} tends to increase for $y_\eta > 10$ and both v'_{rms} and w'_{rms} decrease in the whole channel width (see (a) in the figures). In other words, the flow at high $DR\%$ is prone to become anisotropic turbulence. In such case, the Reynolds shear stress also becomes much small in the near-wall region (see Fig. 7), and it results in the high $DR\%$ as suggested by Eq. (6). Especially, this tendency of fluid D is remarkable and consistent with the discussion above. As seen from Fig. 4(b), profiles of u'_{rms} for the rheologically identical fluids (e.g., constant We_τ and β), do not depend on the Reynolds number. The maximums of v'_{rms} , w'_{rms} and $-u'+v'+$ for non-Newtonian fluids are lower than those of Newtonian fluid, as shown in Figs. 5(b)–7(b). Their peak positions shift away from the wall as Re_τ increases.

Budget of Reynolds stress

The budget terms of Reynolds stress $\overline{u'+u'+}$ in fully-developed channel flow can be expressed as

$$\frac{D}{Dt} \overline{u'+u'+} = P - \varepsilon + \Pi + T + D + E \quad (7)$$

where the terms on the right-hand side are as follows:

$$\text{production} : P = -2\overline{u'+u'+} \frac{\partial \overline{u'+}}{\partial x_k^+}, \quad (8)$$

$$\text{dissipation} : \varepsilon = 2\beta \frac{\partial u'+}{\partial x_k^+} \frac{\partial u'+}{\partial x_k^+}, \quad (9)$$

$$\text{VPG} : \Pi = -2 \left(\overline{u'+} \frac{\partial p'+}{\partial x^+} \right), \quad (10)$$

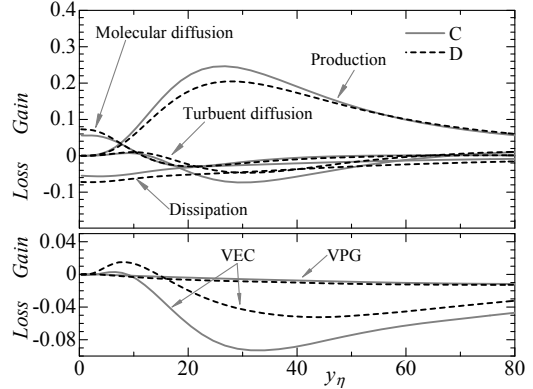


Figure 8: Budget of $\overline{u'+u'+}$ for the almost same $DR\%$ cases.

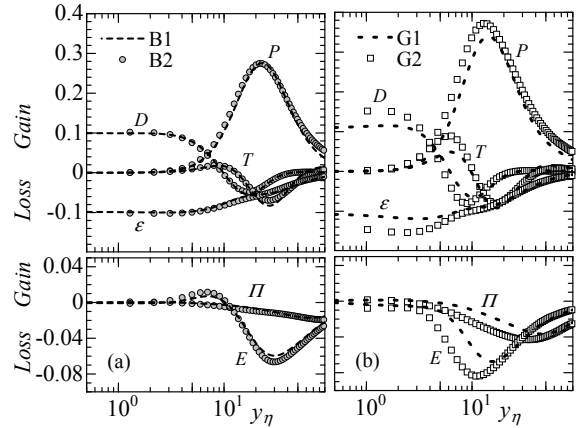


Figure 9: Budget of $\overline{u'+u'+}$: (a) at $Re_\tau = 150$ with high $DR\%$, and (b) at $Re_\tau = 395$ with low $DR\%$.

$$\text{turbulent diffusion} : T = -\frac{\partial}{\partial x_k^+} \overline{u'+u'+} u'_k, \quad (11)$$

$$\text{molecular diffusion} : D = \beta \frac{\partial^2}{\partial x_k^{+2}} \overline{u'+u'+}, \quad (12)$$

$$\text{VEC} : E = 2 \frac{1-\beta}{We_\tau} \left(\overline{u'+} \frac{\partial c_{xk}^+}{\partial x_k^+} \right). \quad (13)$$

Here the VPG and VEC terms denote the velocity pressure-gradient correlation term and viscoelastic contribution term, respectively. The VEC term is an extra term derived from the viscoelastic effect. Figures 8 and 9 show the budget of Reynolds stress $\overline{u'+u'+}$. A difference between Newtonian fluid and non-Newtonian fluid is found in the VPG term corresponding to the pressure strain, also called the redistribution term. It is well-known that the energy transfer from $\overline{u'+u'+}$ to the other directions is attributed to the redistribution term. For non-Newtonian fluid, the VPG term is much smaller than that of Newtonian fluid (not shown here), and hence the relevant flow strengthen the tendency toward anisotropic turbulence.

Although almost same $DR\%$ values are obtained in fluids C and D, their budgets of $\overline{u'+u'+}$ are slightly but significantly different (see Fig. 8). For example, the maximum of the turbulent production in fluid D is much smaller compared to fluid C, which is due to high We_τ . However, the dissipation and the molecular diffusion in fluid D are larger than those of fluid C, which is attributed to low β . These results indicate that high $DR\%$ in fluid D is attributed to the suppressed turbulent production and that in fluid C is

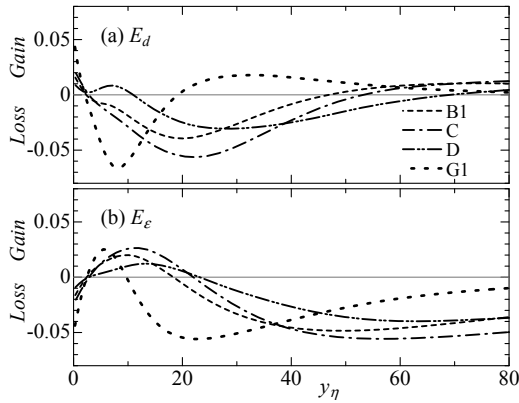


Figure 10: Distribution of viscoelastic contribution.

to the decreased effective viscosity .

It is of interest that, for the high-DR% case, the budget terms are less dependent on the Reynolds number in the whole channel, as shown in Fig. 9(a). On the other hand, for the low-DR% flow as well as a Newtonian-fluid flow, the near-wall values of production, dissipation, molecular diffusion and turbulent diffusion are prone to be increased as Re_τ increases (see Fig. 9(b)). Moreover, the VEC term of the high-DR% fluids (i.e., fluid B1, B2, C, D) works as a gain of turbulent energy in the near-wall region ($y_\eta \approx 10$), whereas it works as a dissipation in the whole area for the low-DR% cases (fluids G1 and G2).

Flow topology and viscoelastic contribution

In order to discuss the viscoelastic contribution in more detail, the VEC term of Eq. (13) is divided to the viscoelastic diffusion E_d and the work by viscoelastic stress E_ϵ .

$$E = E_d - E_\epsilon, \tag{14}$$

viscoelastic diffusion:

$$E_d = 2 \frac{(1-\beta)}{We_\tau} \frac{\partial}{\partial x_k^+} \overline{u'^+ c_{xk}^+}, \tag{15}$$

work by viscoelastic stress:

$$E_\epsilon = 2 \frac{(1-\beta)}{We_\tau} \left(\overline{c_{xk}^+ \frac{\partial u'^+}{\partial x_k^+}} \right). \tag{16}$$

The second term can be interpreted as a dissipation rate from the kinetic energy to the elastic energy. Regarding these two terms, results in several cases are shown in Fig. 10. The E_d transfers the turbulent energy of $u'^+u'^+$ from the buffer layer (from $y_\eta = 5$ to 30) and the elastic layer (i.e., up to 60 in the case of fluid D) to the near-wall region or the channel center (see Fig. 10(a)). On the other hand, the E_ϵ dissipates the turbulent energy in almost whole channel; hence this term can be called ‘viscoelastic dissipation’, while the ϵ is called ‘viscous dissipation’ (see Fig. 10(b)). It is worth noting that, for high DR% (such as fluids B–D), $-E_\epsilon$ becomes positive at the near-wall region of $y_\eta = 5$ –20. It implied that, in this region, there exists a fraction of the elastic energy, which is accumulated at the outer region ($-E_\epsilon < 0$ at $y_\eta > 20$) and backward transferred to the turbulent kinetic energy. Moreover, both E_d and E_ϵ are found to be dramatically dependent on We_τ and β and not scaled by the effective viscosity nor outer scale such as δ .

Figure 11 shows the instantaneous field of $-E_\epsilon$ and the velocity vector in an arbitrarily chosen cross-section of (y, z)

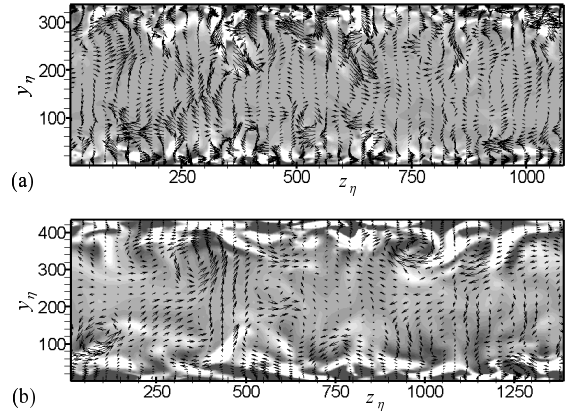


Figure 11: Instantaneous velocity vector and contour of $-E_\epsilon$ in (y, z) -plane for (a) fluid G1, (b) fluid B1: black, $-E_\epsilon > 0.06$; white, $-E_\epsilon < -0.06$. Vectors indicate (v', w')

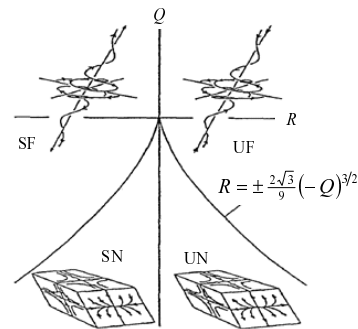


Figure 12: Topology classification of three-dimensional flow pattern, in the Q-R plane. From Soria *et al.*(1994).

plane. Note that the axes are non-dimensionalized by the effective viscosity. In Fig. 11(a), we can observe a number of eddies near the walls, especially in the buffer layer, which has been widely accepted for the Newtonian fluid. For fluid B1 with high DR%, near-wall eddy structures are suppressed and only rather large-scale structures, which extends to the channel center, can be found. Moreover, the region of $-E_\epsilon > 0$ is observed not only at the near-wall region but also at the outer region, and coincides well with the location of a quasi-streamwise vortex, indicating some relationship between the viscoelastic contribution and the local flow topology.

Topological methods are useful in the description of flow fields with large data sets generated by DNS. Chong *et al.* (1990) have carried out a classification of the various types of three-dimensional flow patterns. This classification method is based on the structure in the space of invariants of the velocity gradient tensor \mathbf{A} . The eigenvalues of \mathbf{A} satisfy the characteristic equation. The second and third invariants are given by

$$Q = \frac{1}{2} (\text{trace}[\mathbf{A}]^2 - \text{trace}[\mathbf{A}^2]). \tag{17}$$

$$R = -\det[\mathbf{A}]. \tag{18}$$

Note here that the first invariants is equivalent to Eq. (1). The solutions to the characteristic equation at each point determine the local, linearized flow pattern. Four local-flow topologies, which can occur in an incompressible flow, are determined by the invariants (Q, R) , as given in Fig. 12. The four classifications are unstable focus/contracting (UF), stable focus/stretching (SF), stable node/saddle/saddle (SN), and unstable node/node/saddle (UN), respectively (reading

Table 3: Relation between viscoelastic dissipation, $-E_\varepsilon$, and local-flow pattern defined by topological classification at several wall-normal positions for fluids B1, B2 and G1. Here (+) and (-) indicate $-E_\varepsilon > 0$ and $-E_\varepsilon < 0$, respectively. The values are indicated in percentage, and the boldface represents the most dominant flow pattern in each height.

	$-E_\varepsilon$	$y_\eta = 5$		$y_\eta = 30$		$y_\eta = 94$	
		(+)	(-)	(+)	(-)	(+)	(-)
B1	SF	42	35	46	31	44	36
	UF	30	37	34	42	37	34
	UN	15	16	13	20	13	23
	SN	13	12	7	7	6	7
B2	SF	40	35	41	33	40	36
	UF	32	36	35	42	32	34
	UN	15	17	17	18	20	23
	SN	13	12	7	7	8	8
G1	SF	51	34	34	37	37	38
	UF	24	38	31	34	30	34
	UN	16	16	25	22	23	19
	SN	8	10	10	7	10	9

from top right corner counter-clockwise in the figure). In concrete terms, SN is uniaxial elongation and biaxial compression, UN is biaxial elongation and uniaxial compression, and both UF and SF indicate vortex.

Table 3 shows percentages of each flow pattern (topology) at $y_\eta = 5, 30$ and 94 for three kinds of fluids. In all cases, there is observed a correlation between $-E_\varepsilon$ and the flow topology: if $-E_\varepsilon > 0$, SF is dominant; if $-E_\varepsilon < 0$, UF is dominant, implying that the vortex stretching and compressing can be related with gain and loss of the elastic energy, respectively. It indicates that the relation is satisfied in the energy-gain region (in Fig. 10(b)) so that this region dominates vortex. This tendency is apparent for a high $DR\%$ case. For instance, in the cases of fluids B1 and B2, this relation maintains at $y_\eta = 30$.

CONCLUSION

We performed DNS on the turbulent channel flow of viscoelastic fluids using the Giesekus constitutive equation at two Reynolds number $Re_\tau = 150$ and 395 , and systematically investigated drag-reducing flows with various values of the Weissenberg number and the viscosity ratio. Moreover, the viscoelastic dissipation term is studied with emphasis on its relation to turbulent flow topologies related to the invariants of the velocity gradient tensor. The budget of the turbulent intensity is also discussed focusing on the “viscoelastic dissipation $-E_\varepsilon$ (from turbulent kinetic energy to elastic energy)”, which is absent in Newtonian-fluid flow. The main results may be summarized as follows:

1. High drag reduction can be achieved by suppression of the turbulent production for high Weissenberg-number fluid, and/or by decrease of the effective viscosity.
2. Positive $-E_\varepsilon$ gives rise to vortex stretching that produces turbulent energy, whereas a negative one causes vortex compression (energy loss).
3. For a high drag-reducing flow, the viscoelastic contribution and its relationship to the local-flow topology are significant in the outer layer as well as in the inner near-wall region.

ACKNOWLEDGEMENTS

The present computations were performed with the use of supercomputing resources at Cyberscience Center at Tohoku University. This work was conducted in Research Center for the Holistic Computational Science (Holcs). The fourth author expresses appreciation to the support by the National Science Foundation of China (No. 50876114, No. 50506017 and No. 10602043), SRF for ROCS, SEM the Specialised Research Fund for the Doctoral Programme of Higher Education of China (No. 20050425006) and the Key Project of Chinese Ministry of Education (No. 106034).

REFERENCES

Chong, M. S. *et al.*, 1990, “A general classification of three-dimensional flow fields,” *Phys. Fluids*, **2**, 765–777.

Dean, R. D., 1978, “Reynolds number dependence of skin friction and other bulk flow variables in two-dimensional rectangular duct flow,” *J. Fluids Eng.*, **100**, 215–223.

Dimitropoulos, C. D. *et al.*, 1998, “Direct numerical simulation of viscoelastic turbulent channel flow exhibiting drag reduction: effect of the variation of rheological parameters,” *J. Non-Newton. Fluid Mech.*, **79**, 433–468.

Fukagata, K. *et al.*, 2002, “Contribution of Reynolds stress distribution to the skin friction in wall-bounded flows,” *Phys. Fluids*, **14**, L43–L76.

Giesekus, H., 1982, “A simple constitutive equation for polymer fluids based on the concept of deformation-dependent tensorial mobility,” *J. Non-Newton. Fluid Mech.*, **11**, 69–109.

Housiadas, K. D. and Beris, A. N., 2004, “An efficient fully implicit spectral scheme for DNS of turbulent viscoelastic channel flow,” *J. Non-Newton. Fluid Mech.*, **122**, 243–262.

Soria, J. *et al.*, 1994, “A study of the fine-scale motions of incompressible time-developing mixing layers,” *Phys. Fluids*, **6**, 871–884.

Sureshkumar, R. *et al.*, 1997, “Direct numerical simulation of the turbulent channel flow of a polymer solution,” *Phys. Fluids*, **9**, 743–755.

Toms, B.A., 1948, “Some observations on the flow of linear polymer solutions through straight tubes at large Reynolds numbers,” *Proc. First Int. Congress on Rheology*, pp. 135–141.

Den Toonder, J. M. J., 1997, “Drag reduction by polymer additives in a turbulent pipe flow: numerical and laboratory experiments,” *J. Fluid Mech.*, **337**, 193–231.

Virk, P.S., 1971, “Drag reduction in rough pipes,” *J. Fluid Mech.*, **45**, 225–246.

Wei, J. *et al.*, 2006, “Rheological characteristics and turbulent friction drag and heat transfer reductions of a very dilute cationic surfactant solution,” *J. Heat Transfer*, **128**, 977–983.

White, C. M. and Mungal, M. G., 2008, “Mechanics and prediction of turbulent drag reduction with polymer additives,” *Annu. Rev. Fluid Mech.*, **40**, 235–256.

Yu, B. and Kawaguchi, Y., 2004, “Direct numerical simulation of viscoelastic drag-reducing flow: a faithful finite difference method,” *J. Non-Newton. Fluid Mech.*, **116**, 431–466.

Yu, B. and Kawaguchi, Y., 2006, “Parametric study of surfactant-induced drag-reduction by DNS,” *Int. J. Heat and Fluid Flow*, **27**, 887–894.

Yu, B. *et al.*, 2004, “Numerical and experimental investigation of turbulent characteristics in a drag-reducing flow with surfactant additives,” *Int. J. Heat and Fluid Flow*, **25**, 961–974.